THE OHIO STATE UNIVERSITY

NON-EQUILIBRIUM THERMODYNAMICS LABORATORY

SAND2019-3404PE

Interrogation of Plasma Discharges in Reacting Molecular and Supersonic Environments via Advanced Spectroscopic and Imaging Diagnostics

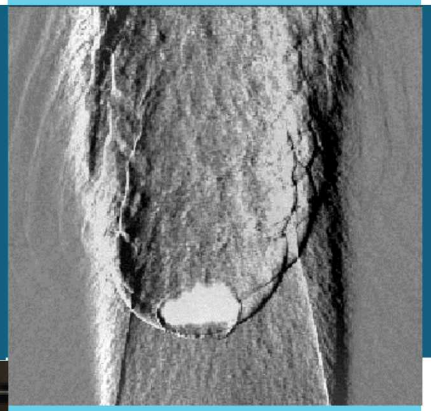

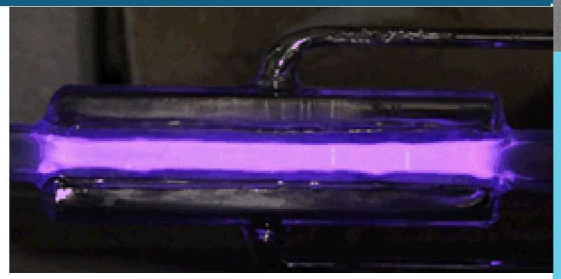

Caroline Winters, PhD

April 1st, 2019, Vanderbilt University

Sandia National Laboratories is a multimission laboratory managed and operated by National Technology & Engineering Solutions of Sandia, LLC, a wholly owned subsidiary of Honeywell International Inc., for the U.S. Department of Energy's National Nuclear Security Administration under contract DE-NA0003525.

SAND2019-0085 C

Nonequilibrium plasmas

Reduced Electric Field $\sim \frac{E}{N}\ (Vcm^2)$

↓

- Electron energy
- Input energy partition
- Rates of electron impact processes

low to mid E/N

(1) O_2 vibrational excitation
(2) O_2 and N_2 rotational
(3) Elastic losses
(4) N_2 vibrational excitation

Input Energy Partition vs. Reduced Electric Field

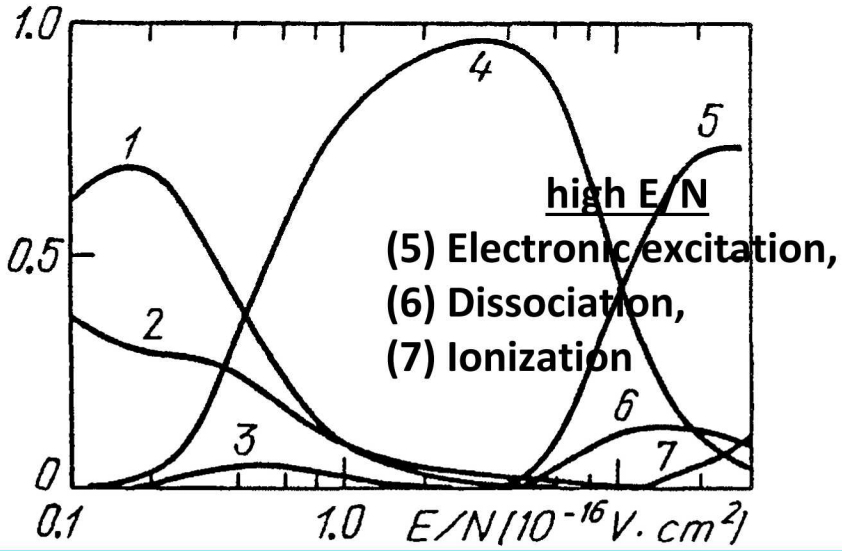

(Yu. Raizer, Gas Discharge Physics, Springer, 1991)

Transient plasmas (ns pulse duration):

Critical issues / concerns:

1. Plasma stability at high pressures (rapid thermalization ⇒ discharge filamentation)
2. Scarcity of experimental data at controlled, well-characterized plasma conditions
3. Validation of kinetic models, developing quantitative predictive capability

Plasma-assisted combustion

Ignition and combustion become unstable at the conditions of:

- Lean equivalence ratios $\phi = (F/A) / (F/A)_{stoichiometric}$
- High flow velocities in combustor
- Low pressures in combustor

Capabilities provided by non-equilibrium plasmas:

- Efficient generation of a pool of highly reactive radical species → Not just a temperature rise; (Uddi et al. 2009, Stancu et al. 2010, & Schmidt et al. 2015)
- Radicals react rapidly with fuel, even at low temperatures; (Yin, et al. 2013, Tsolas, et al. 2016)

Effect of plasma-generated radicals on fuel-air flows (prior ~10-20 years):

- Ignition time varies inversely with numbers of ns-pulses (Yin, et al. 2013)
- Reduction of ignition threshold at $T_0 < T_{thermal}$ (up to 100-200 K, plasma flow reactors) (Yin, et al. 2013)
- Reduction of lean flammability limit (up to $\Delta\phi/\phi \sim 10\%$, premixed turbulent flames) (Pilla, et al. 2006)

Designs for "0D" plasma flow reactor

Liquid Metal-Quartz Electrodes

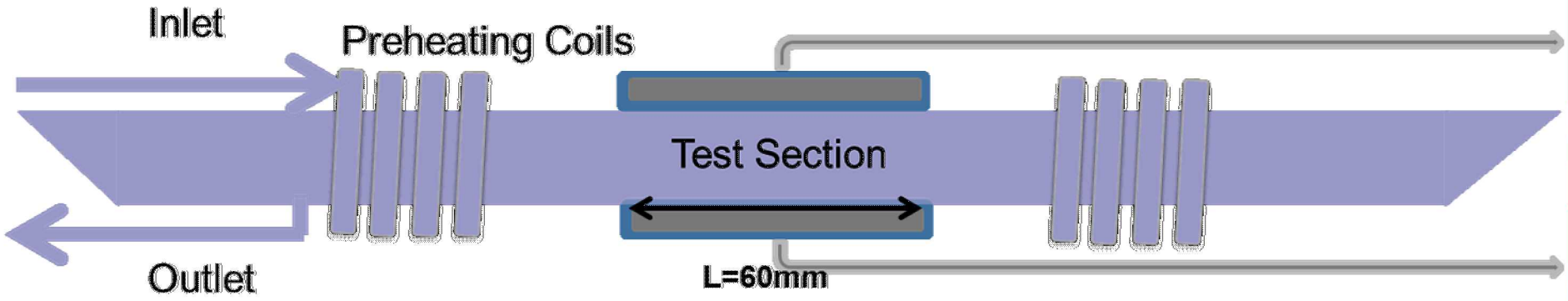

Side view: single shot ICCD plasma image

End view

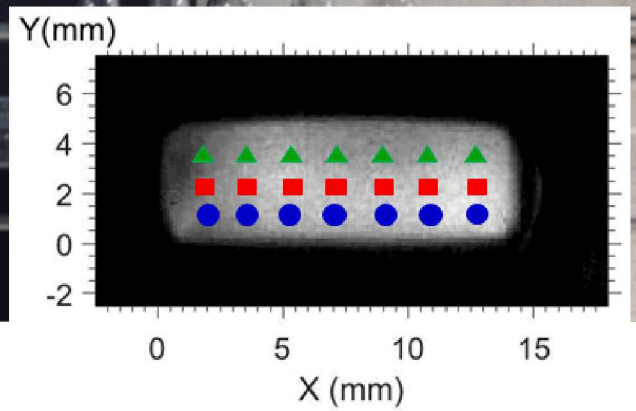

T_0= 500 K, P= 300 Torr
10 kHz, 50th pulse, 1% O_2- Ar

- [$Ar(3p^54s)$] distribution used as plasma uniformity metric
- Tunable Diode Laser Absorption Spectroscopy, the $1s_5 \rightarrow 2p_7$ transition
- Variation in a 1% O_2-Ar mixture, P= 300 Torr, T_0= 500 K is ~10%

In-situ laser diagnostics for radical species measurements

Two-photon Laser Induced Fluorescence (TALIF)

H radical

Calibration via Krypton TALIF

Quenching taken from femtosecond TALIF measurements

(Schmidt, et al. 2015)

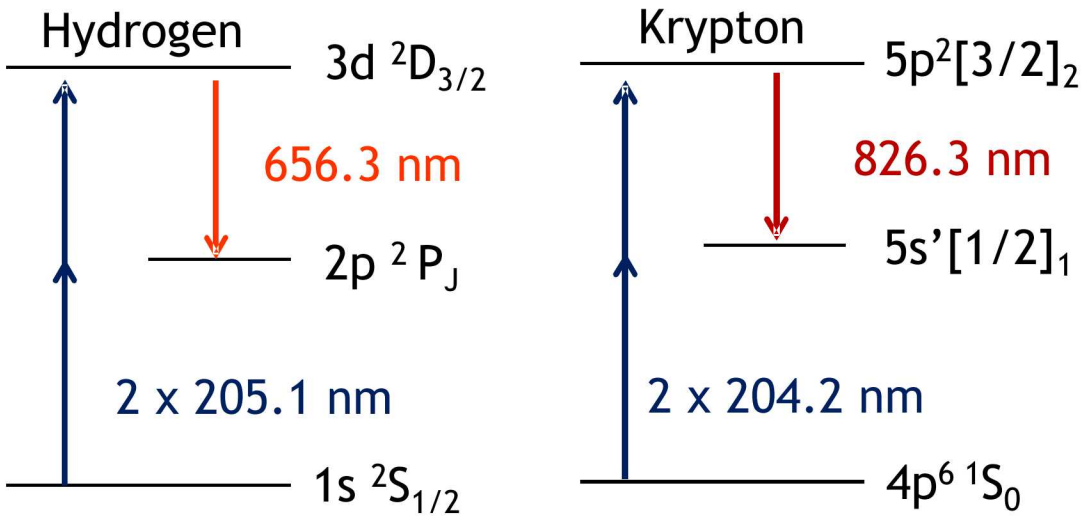

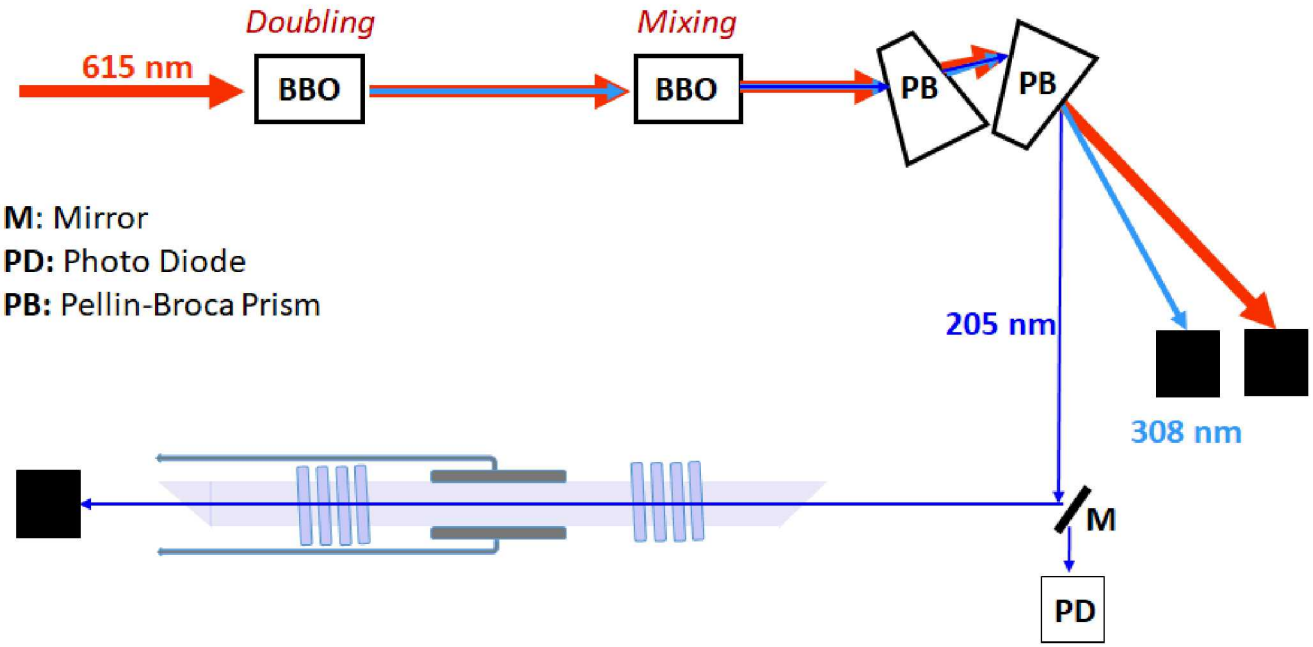

In-situ laser diagnostics for radical species measurements

Two-photon Laser Induced Fluorescence (TALIF)

O radical

Calibration via Xenon TALIF

Quenching taken from femtosecond TALIF measurements

(Schmidt, et al. 2015)

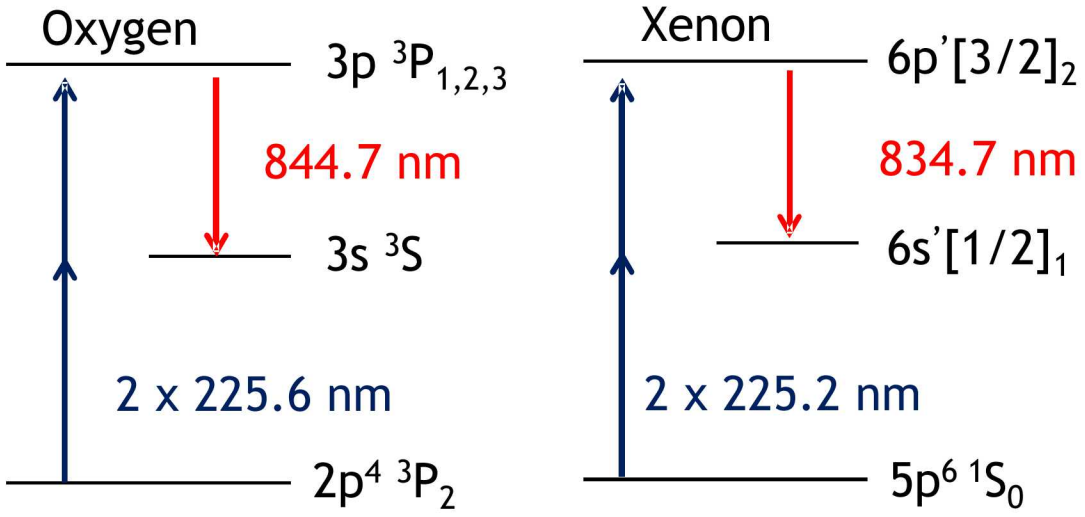

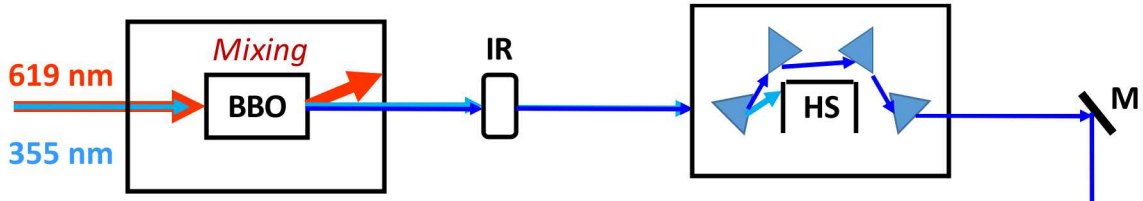

M: Mirror
IR: Iris
PD: Photo Diode
HS: Harmonic Separator

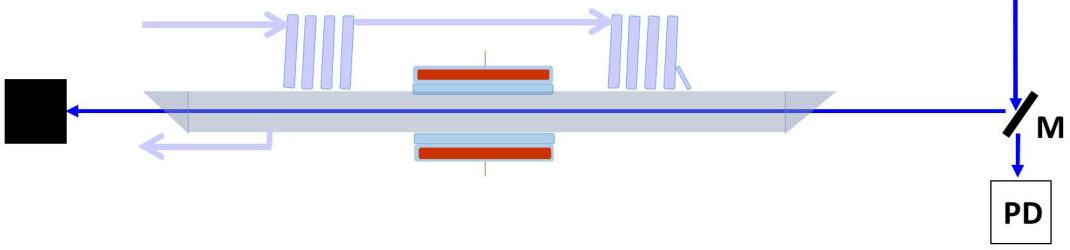

Nanosecond pulsed discharge in 'burst' mode

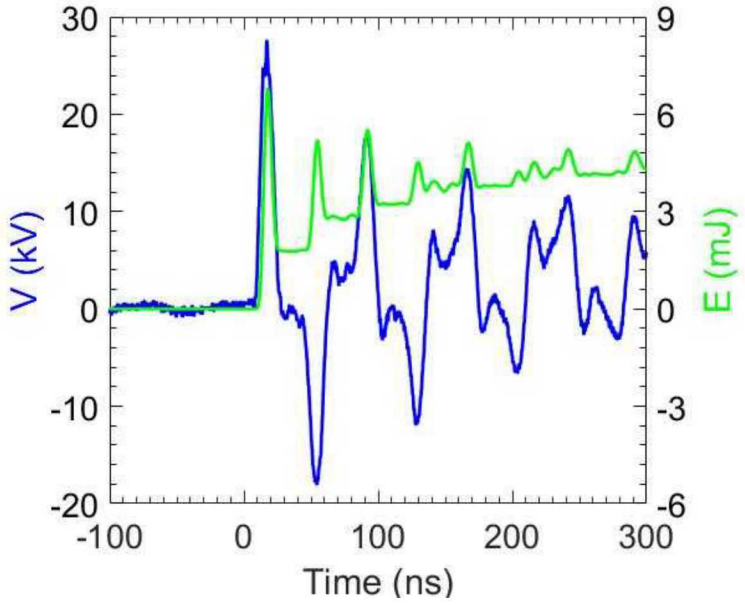

T_0= 500 K, P= 300 Torr
20 kHz, 75th pulse, 1% O_2- Ar

Pulser produces a rapid "burst" of:
25-75 pulses
Repetition rate = 10-20 kHz
FWHM of ~ 5 ns
Peak Voltage of ~ 30kV

Burst is repeated at Δt =10 Hz to match laser repetition rate.

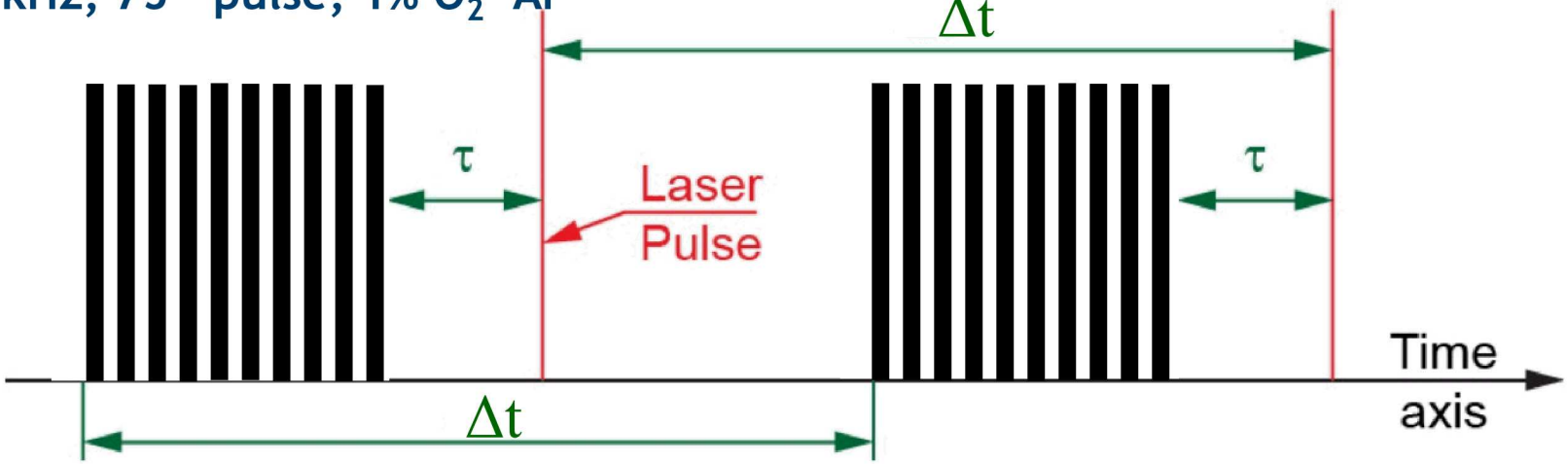

Insight into radical production

[H] produced with varying pulse burst size

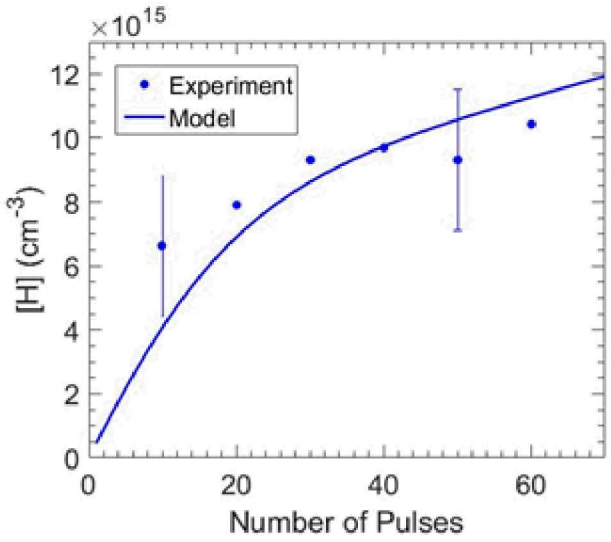

T_0= 500 K, P= 300 Torr,
10 kHz, 1% H_2-Ar

[O] produced with varying pulse burst size

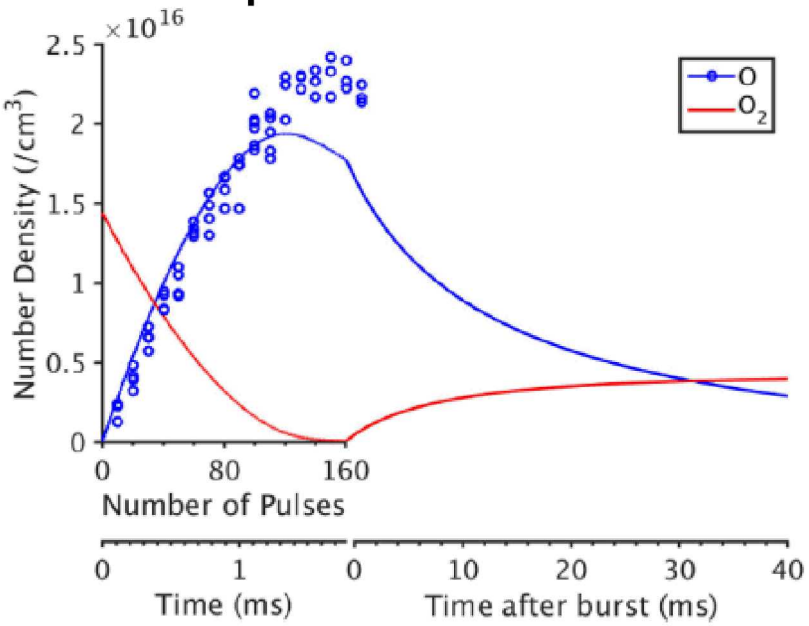

20 kHz, 1% O_2-Ar

- Kinetic modeling predicts 80% of the E_{CDP} → Ar excitation
- 70% of that ($0.8E_{CDP}$) → dissociative quenching of Ar*
- In other terms, **56% of the initial E_{CDP} → dissociation**

$$Ar + e^- \rightarrow Ar^* + e^-$$

$$Ar^* + H_2 \rightarrow Ar + H + H$$

$$Ar^* + O_2 \rightarrow Ar + O + O$$

~~100% dissociation of O_2 measured after ~110 pulses~~
Measurements after 1120 pulses subject to EMI
Overall good agreement between measurements and predictions

Time-resolved H atom measurements

[H] decay after last pulse

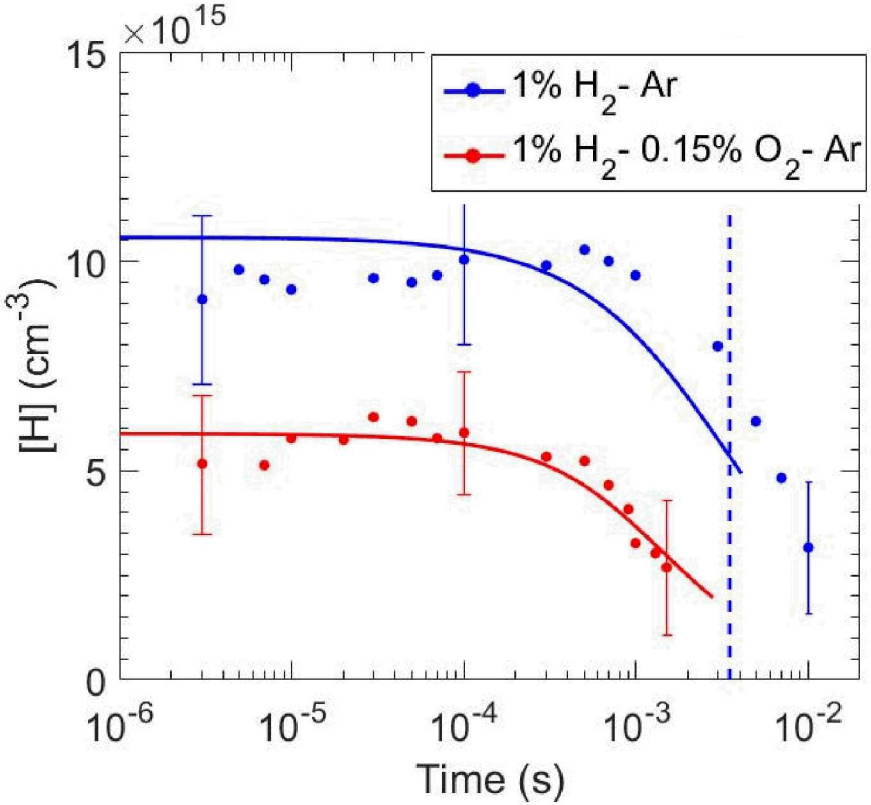

T_0= 500 K, P= 300 Torr
20 kHz, 25 pulses

H TALIF Line Images

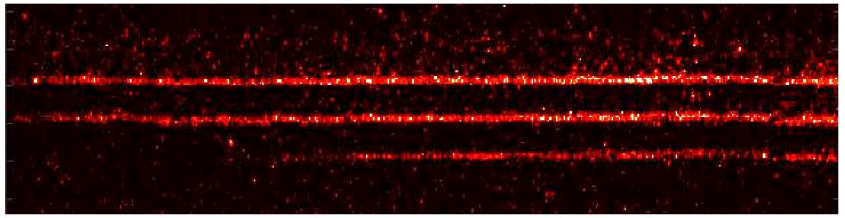

- Good agreement between data and predictions
- H atom decay is overpredicted in H_2-Ar mixture
  - Similar behavior to fs-TALIF experiments (Schimidt, et al. 2015)
- Convection is additional decay mechanism at long enough time scales

Time-resolved O atom measurements

[O] decay after last pulse

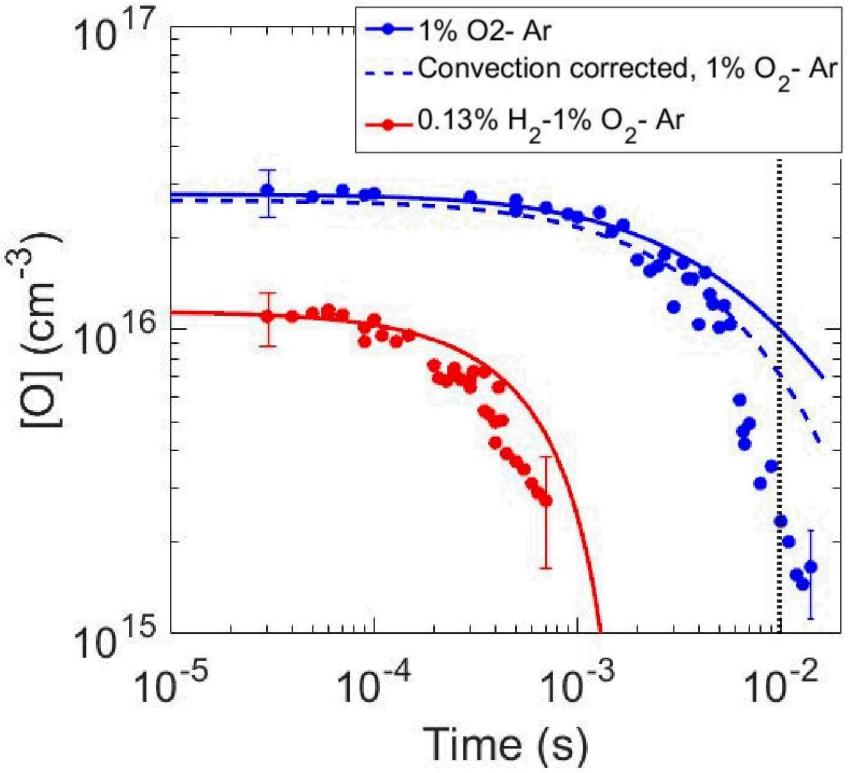

T_0= 500 K, P= 300 Torr
20 kHz, 75 pulses

- Good agreement between data and predictions
- O atom decay is underpredicted in O_2-Ar mixture
  - Inclusion of convection improves agreement in O atom decay rate
- Addition of H_2, reduces peak [O] produced during the discharge burst and increases the decay rate
- In the O_2-Ar mixture, ≈40% of initial O_2 is dissociated during the discharge burst

0D Boltzmann+/Chemkin model methodology

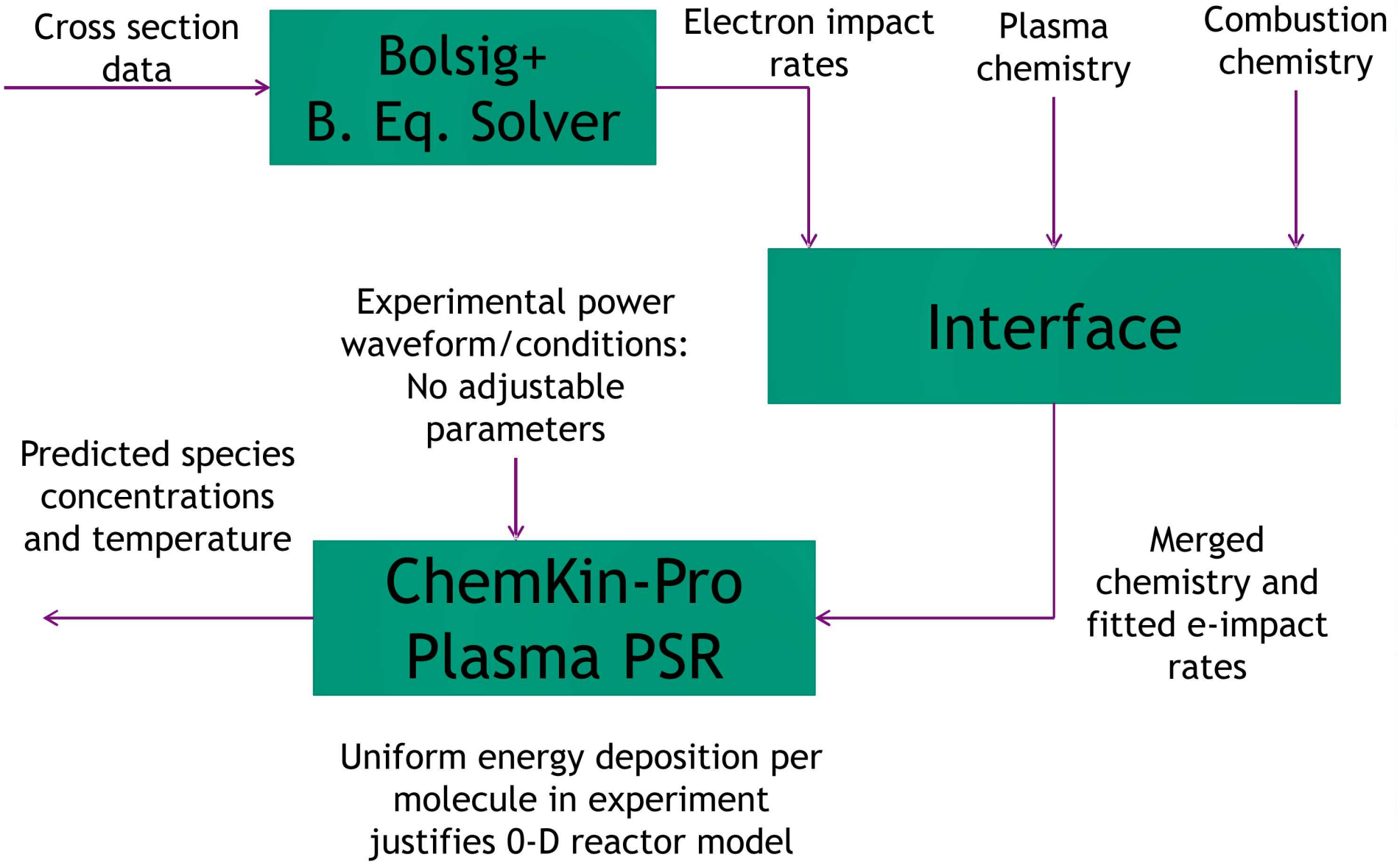

Insight into reaction kinetics

Number density predictions of dominant species, after the burst

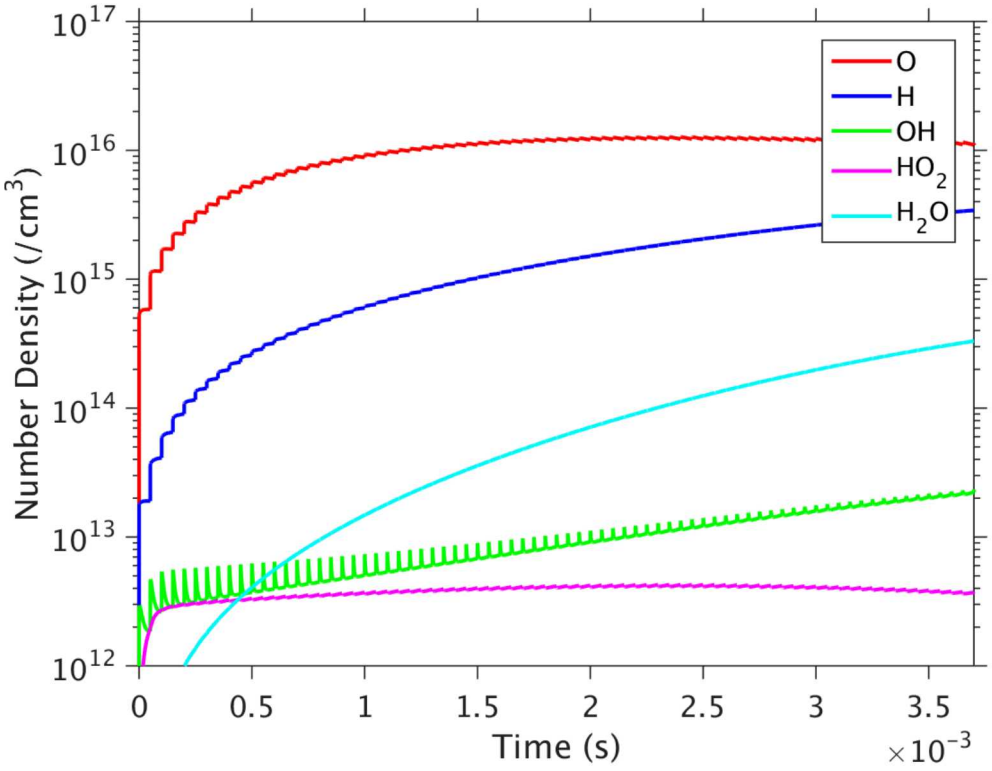

T_0= 500 K, P= 300 Torr
20 kHz, 75 pulses
0.13% H_2-1% O_2-Ar

Kinetic modeling predicts in a H_2–O_2 -Ar mixture:

Reduced Mechanism for radical decay

H atoms recombine with O_2,

$$H + O_2 + Ar \rightarrow HO_2 + Ar$$

$$O + OH \rightarrow H + O_2$$

Additional H atom reaction with HO_2 forms OH,

$$H + HO_2 \Rightarrow 2OH$$

O atoms react with OH,

$$H + O_2 + Ar \rightarrow HO_2 + Ar$$

$$O + H_2 \rightarrow OH + H$$

Estimated chain length is $\frac{H_2O}{[H][O]} \sim 1.1$

→Chain branching reactions are negligible

Conclusions of this work

- Measurements of [H] and [O] by TALIF provide quantitative insight into reaction kinetics using a "0D" plasma flow reactor
- Atomic radicals are produced by Ar* quenching reactions with H_2 and O_2 (~20% E_{CDP}→ H atom, ~50% E_{CDP}→ O atom)
- At long timescales, the near 0D approximation fails and predictions must account for the convection of the flow
- In low temperature plasma oxidation, chain branching reactions are negligible
- A reduced mechanism demonstrates atomic radical species decay is dependent only the amount of primary radicals produced during the discharge burst

This work was funded by the DOE PSAAP-2 Center
"Exascale Simulation of Plasma-Coupled Combustion"

Nanosecond plasmas for flow actuation

- AC Surface-dielectric barrier discharge (AC-SDBD)
  - Diffuse and uniform plasmas
  - "Ionic wind" generates a body-force coupled with momentum in the external flow; (Corke et al., 2010)
- Arc filaments
  - High temperature, constricted plasmas
  - Flow control via heating → density change in the plasma affects mass balance of the system; (Leonov, 2004 & Webb et al., 2013)
  - Rapid localized heating generates strong compression wave; (Samimy et al., 2007 & Adamovich, 2009)
- Nanosecond pulsed plasma actuators:
  - Must be located at walls or jet exits
  - High repetition rates: $\tau \leq 100$ kHz
  - Strong scaling implications for large volume flows

AC-SDBD interacting with smoke

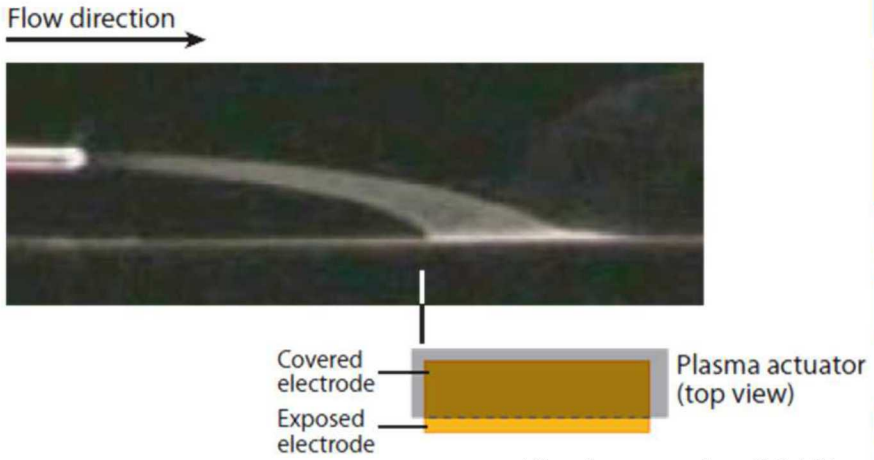

(Corke et al., 2010)

Four DC arc filament discharges interacting with a jet

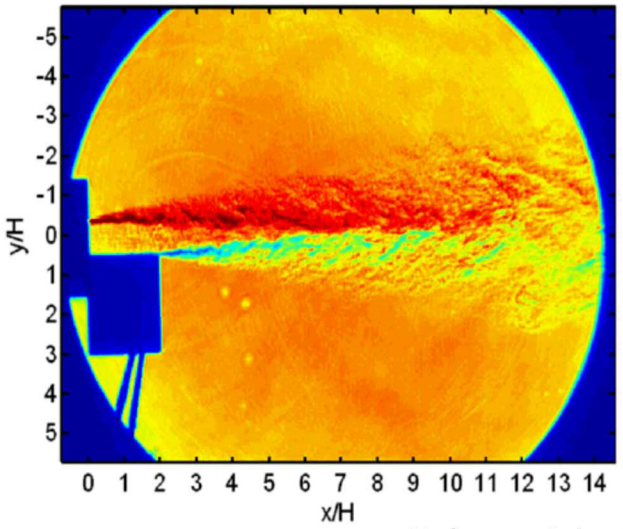

(Adamovich, 2009)

Energy deposition in flows by laser-induced plasmas

- Provides non-intrusive deposition with high energy density
- Rapid implementation allows changes in location, energy, and repetition rate
- Flow interaction time limited by the repetition rate of the laser
- Previous work has successfully implemented laser induced plasmas into supersonic flows
  - Reduce pressure forces on blunt bodies in supersonic flows; [Adelgren et al., 2005]
  - Deflect oblique shocks in supersonic inlets; [Han et al., 2002]

- Relative energy imparted into the flow; [Knight, 2008]

$$\varepsilon = {Q}\Big/{\rho_\infty C_p T_\infty V}$$

- Q: laser pulse energy (kJ)
- ρ_∞: jet exit density (kg/m^3)
- C_p: heat capacity (kJ/kg/K)
- T_∞: jet exit temperature (K)
- V: plasma volume (m^3)

- Previous work have studied laser induced plasmas with ε = 77-2100; [Adelgren et al., 2005]

Explore high-bandwidth effects of supersonic flows on pulse-burst laser-induced plasmas

Determine the conditions to sustain a pulse-burst laser-induced plasma at high Re jets

Experimental design

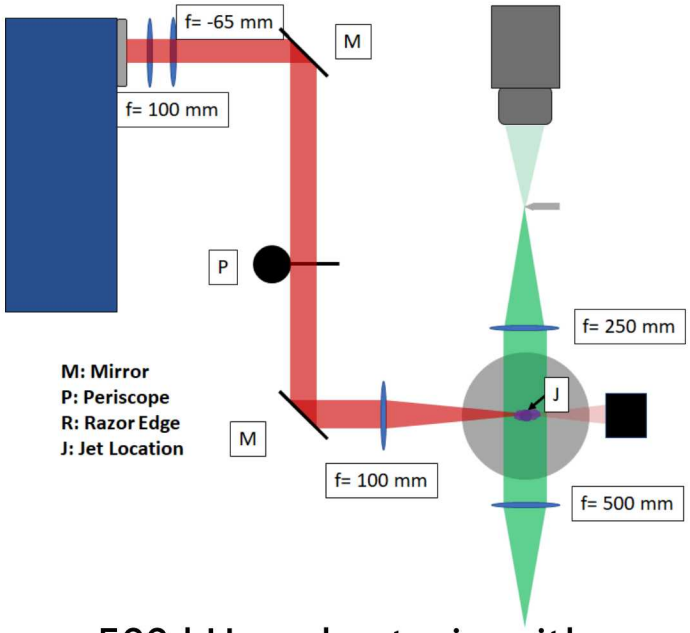

500 kHz pulse train with camera gate

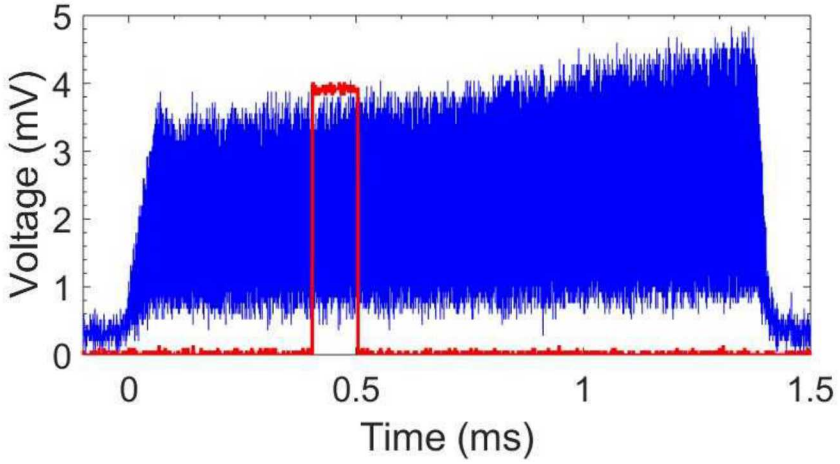

Burst rate: 5- 500 kHz, Burst duration: 1.5-10.5 ms
Total burst energy E ~ 15 J, $\varepsilon \sim 13 - 300$

Imaging of overexpanded, unperturbed jet

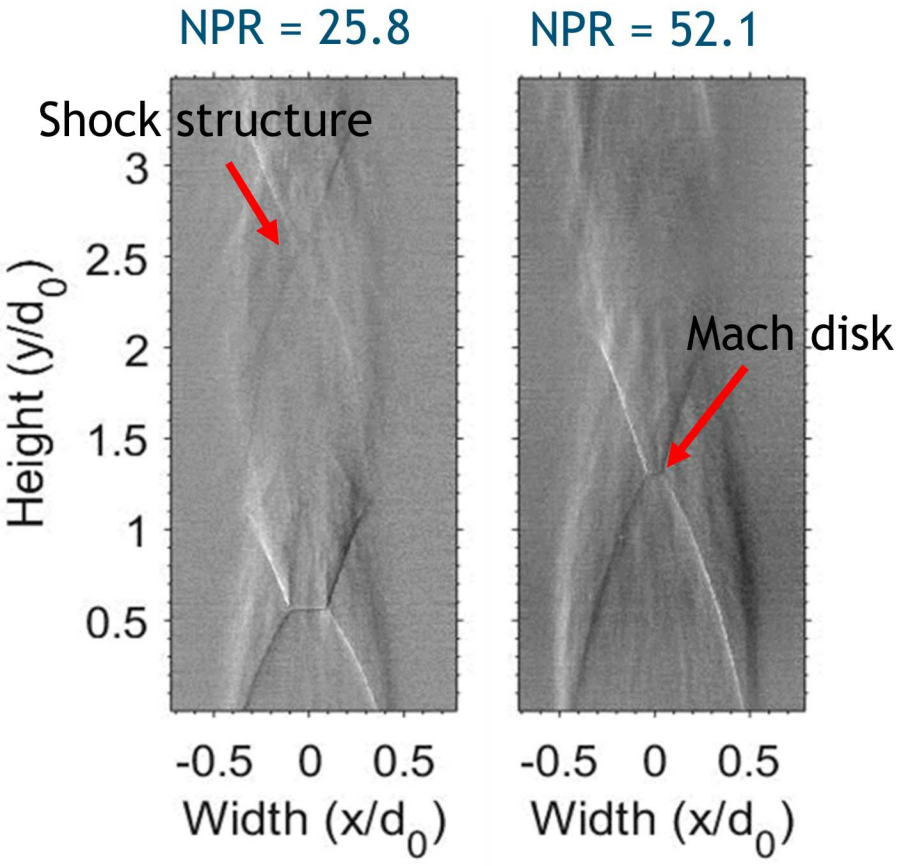

C-D nozzle, M= 3.71
Nozzle pressure ratio (NPR) ~19.5-52.1
T_{exit} = 80 K, v_{exit} = 660 m/s $d_0 = 6\ mm$

Laser-induced plasmas in quiescent air

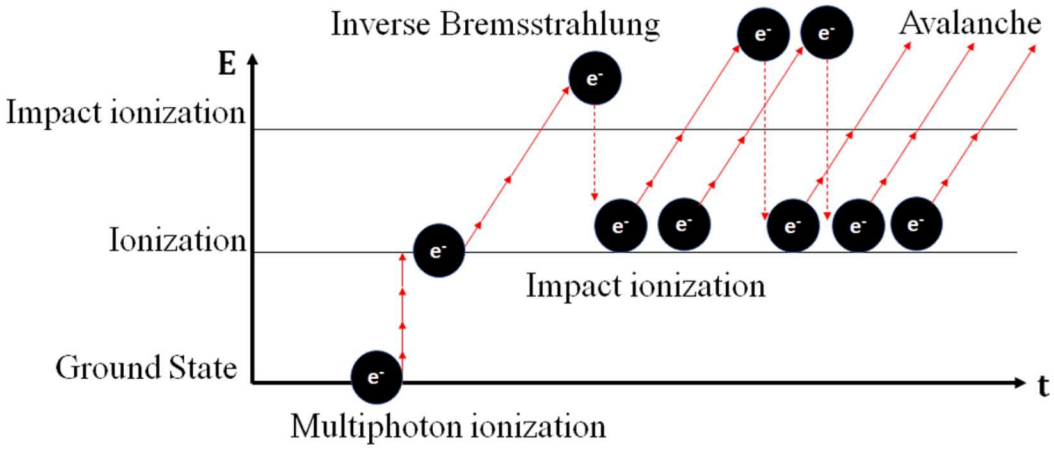

- Formation by two ionization mechanisms
  - Multiphoton → seed electron generation
  - Collisional cascade → electron avalanche
- Vortex formation generates high velocity, hot air jet
- Breakdown in air is stochastic

Plasma-induced blast wave

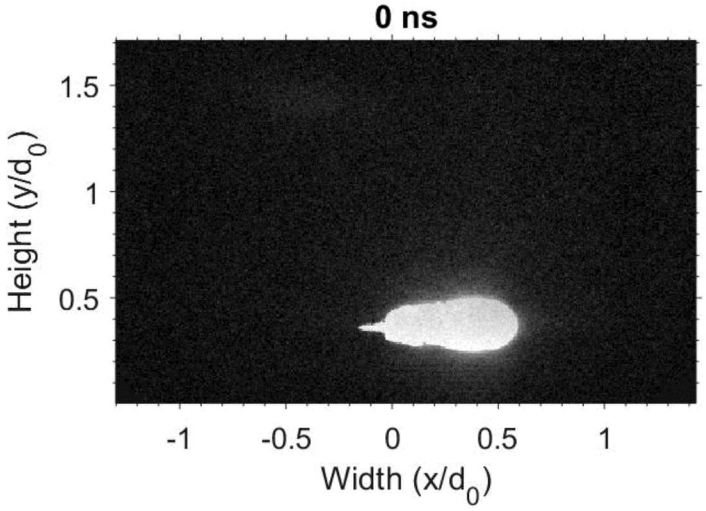

E= 310 mJ/pulse; Frame rate = 5 MHz, τ_{exp} = 10 ns

Core gas dynamics

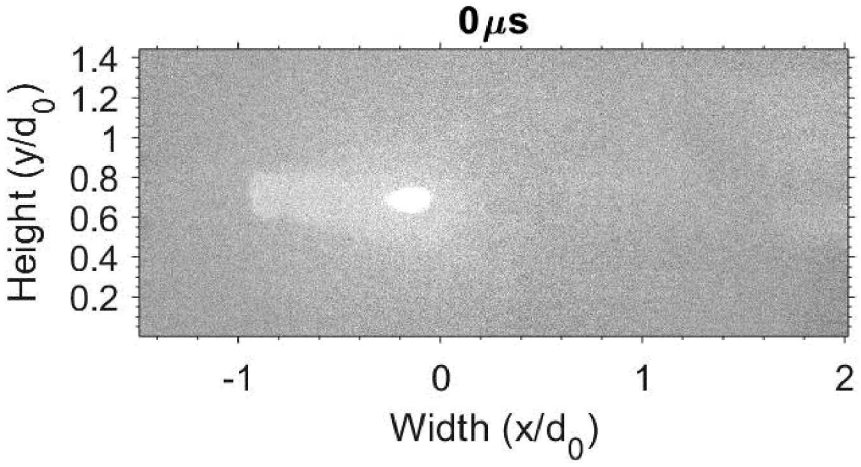

20 kHz burst rate

Frame rate = 60 kHz, τ_{exp} = 1 μs

Interaction between plasma-induced jets and supersonic flows

Location of plasma relative to jet

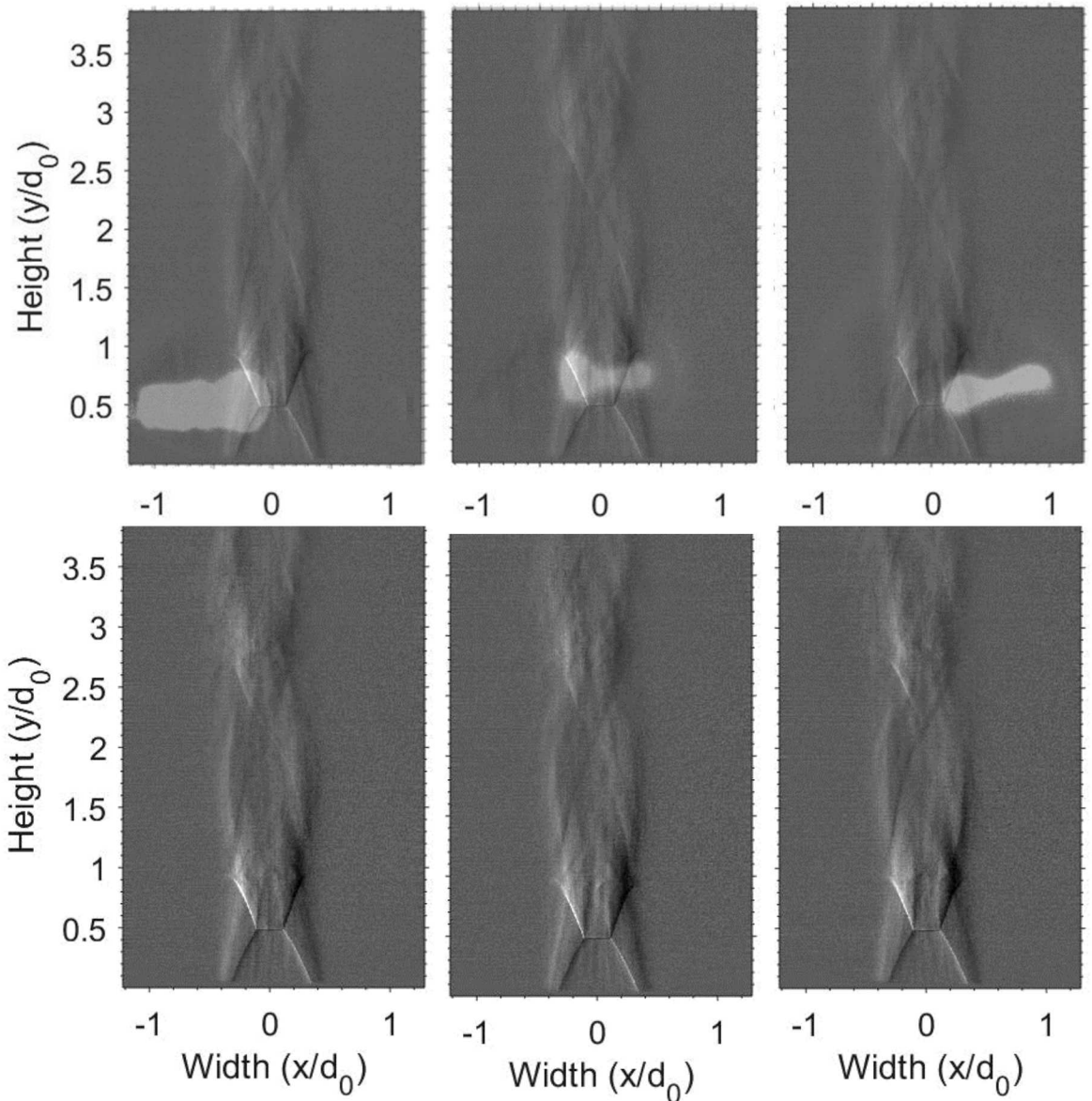

Hot air from plasma

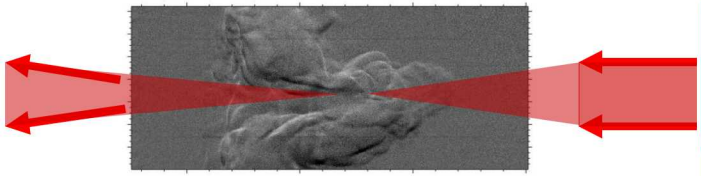

NPR= 19.2, 20 kHz burst rate

Frame rate 30 kHz

- Pushing/suction mechanism
- Collapse of the oblique shock wave
- Mach disk recovery
- Downstream shock structure
- Entrainment of hot gas

Laser pulse energy affect on jet modulation

Location of plasma relative to jet

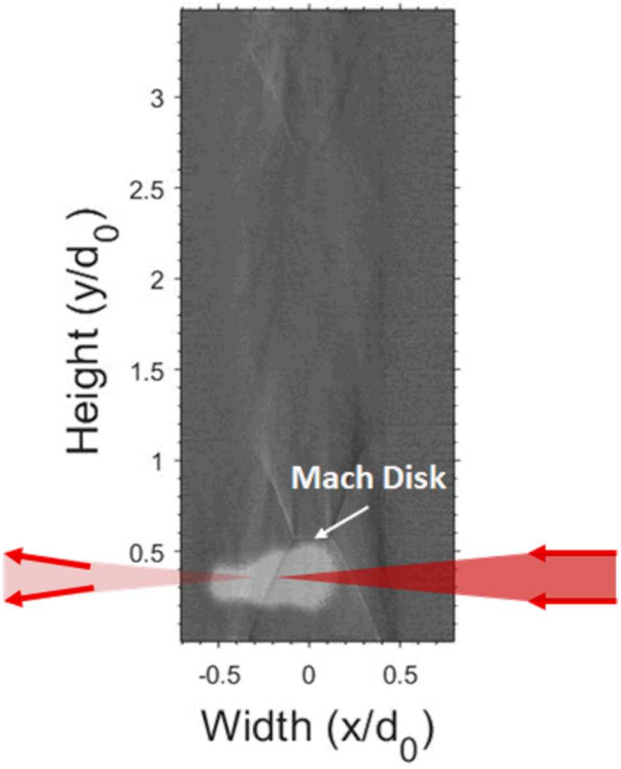

NPR= 25.9, 5 kHz burst rate

Energy variance on jet modulation

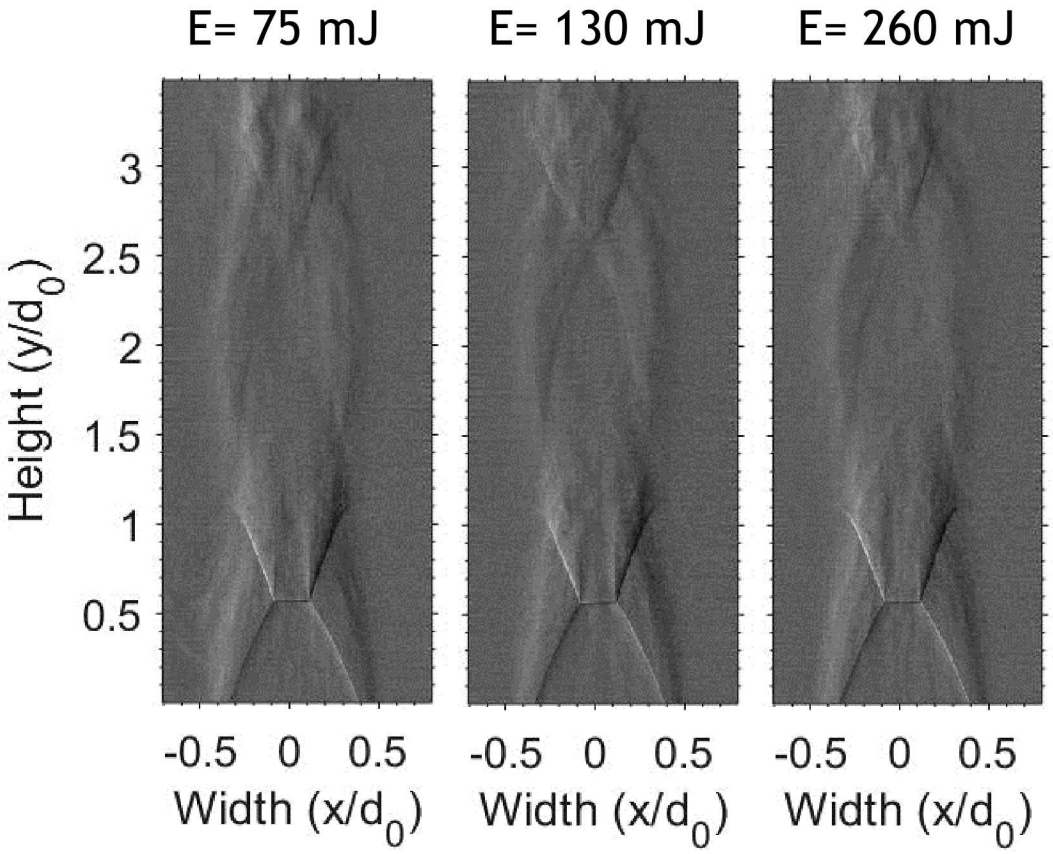

Frame rate 50 kHz, exposure 1 μs

- Low laser pulse energy effects downstream shock structure, not oblique shock waves
- High laser pulse energy is destructive to jet

Increasing laser pulse energy increase plasma volume and jet interaction

Power spectral density analysis of jet modulation by laser pulse

Regions of analysis

PSD analysis

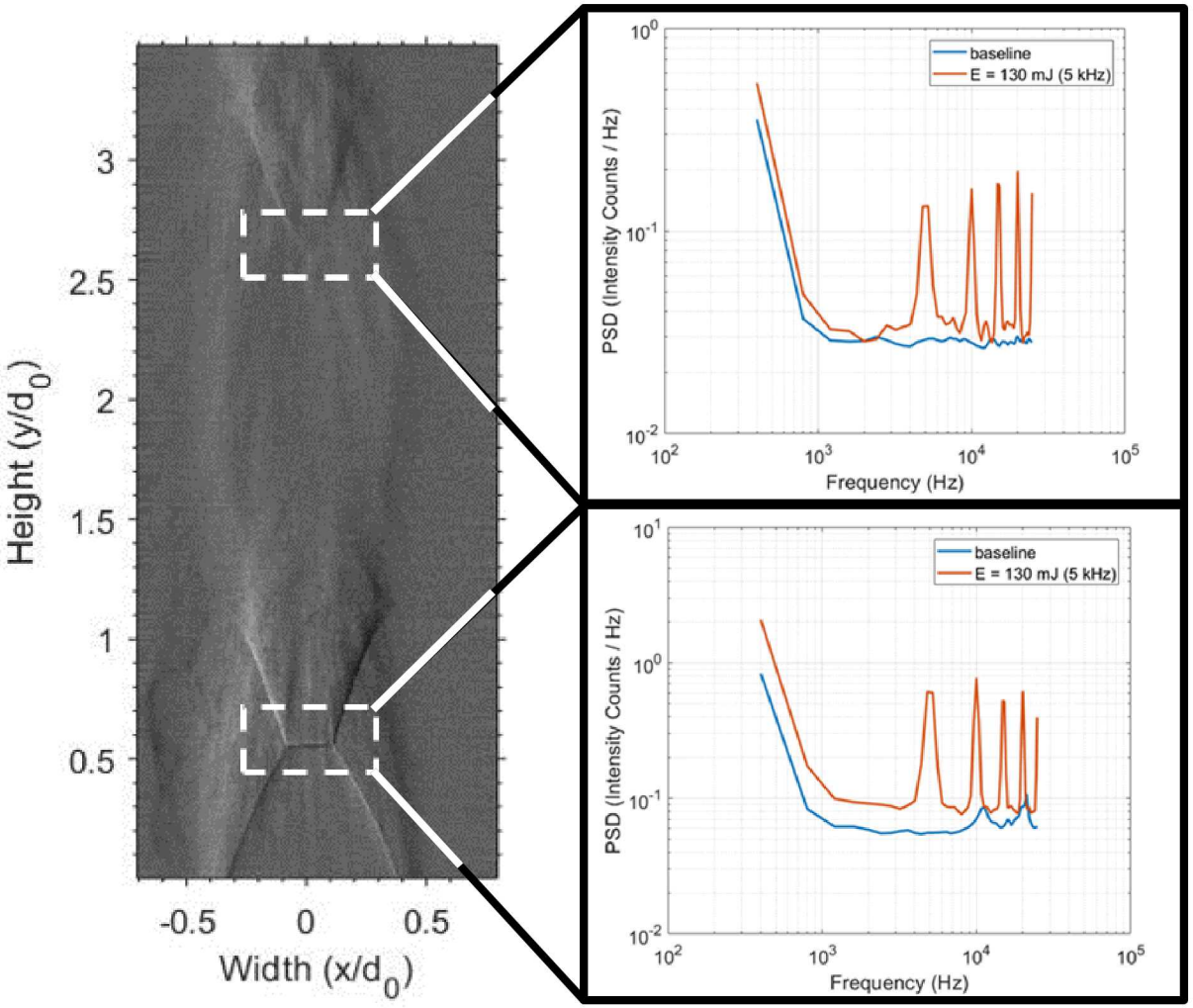

NPR= 25.9, 5 kHz burst rate
E= 130 mJ/pulse

- No analysis below 800 Hz, due to Schlieren noise limitations
- Prominent peaks
  - 5, 10, 10.5, 20, and 20.5 kHz
  - Instantaneous energy deposition
- Peaks a function of laser energy

Jet near and far fields are undulated by the laser-plasma

High repetition-rate breakdown in supersonic flow

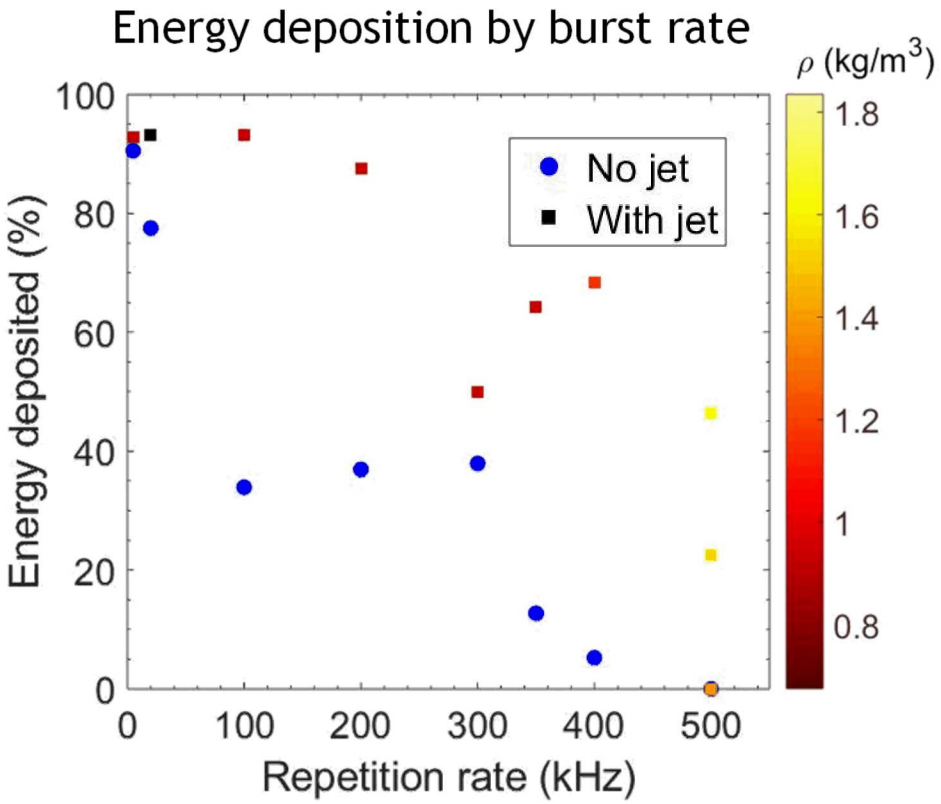

- Stochasticity in pulse-burst laser-induced plasma in quiescent air increases at higher burst rates
- Refresh rate of the supersonic jet sustains breakdown at $\tau < 350$ kHz
- Sustained breakdown at $\tau > 350$ kHz, requires both greater flow and jet exit density

Coupling pulse-burst laser-induced plasma to the supersonic jet reduces stochasticity

High-bandwidth laser-plasma/jet-flow interactions

Unperturbed jet, NPR = 52.1

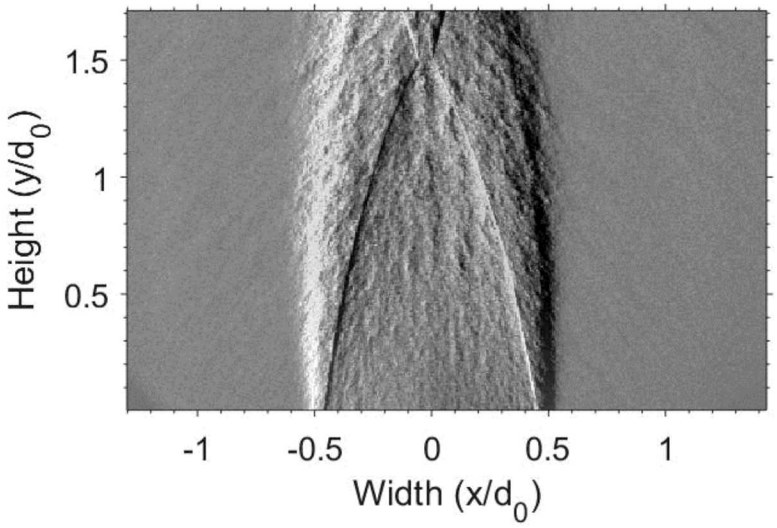

500 kHz burst rate

Frame rate 5 MHz, exposure 10 ns

- High repetition breakdown in the flow
- Permanent jet modulation
- Continuous plasma emission at the jet core
- Shock re-excitation of plasma species

Permanently disrupted jet

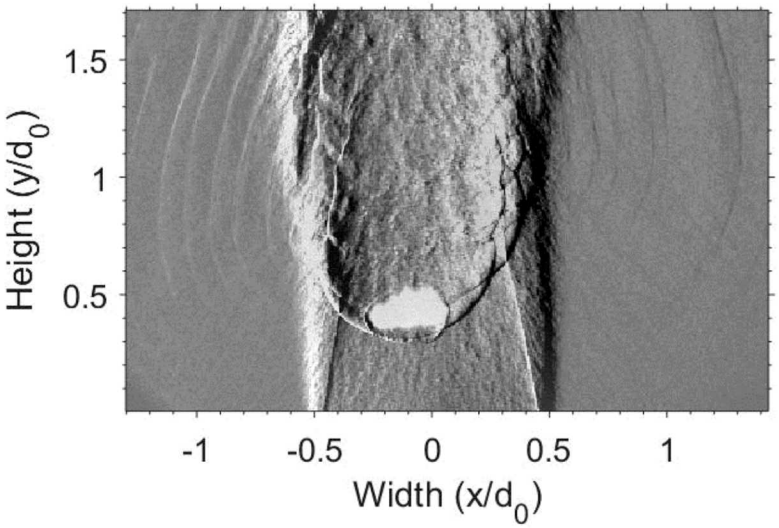

N(II) emission in jet core

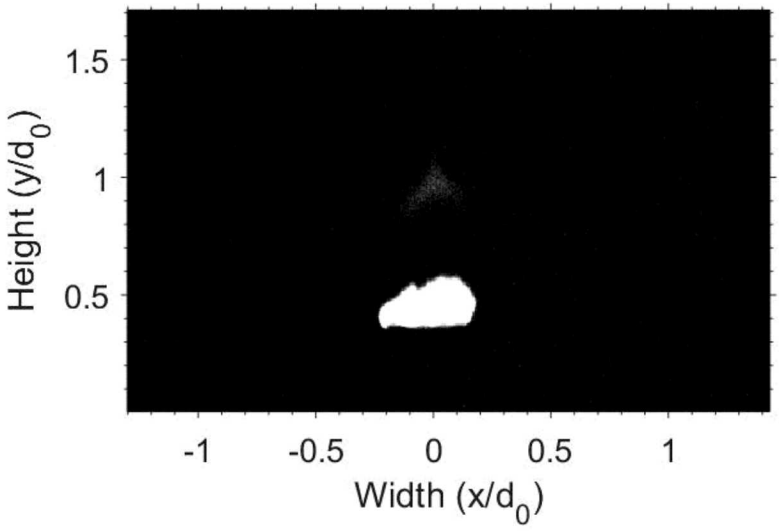

Implications for supersonic plasma ignition

N(II) emission in jet core

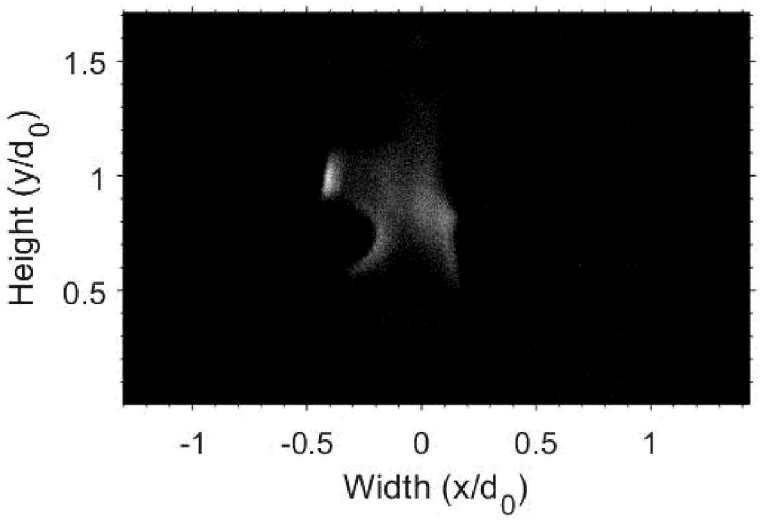

300 kHz burst rate

Frame rate 5 MHz, exposure 100 ns

Repeatability of plasma convection

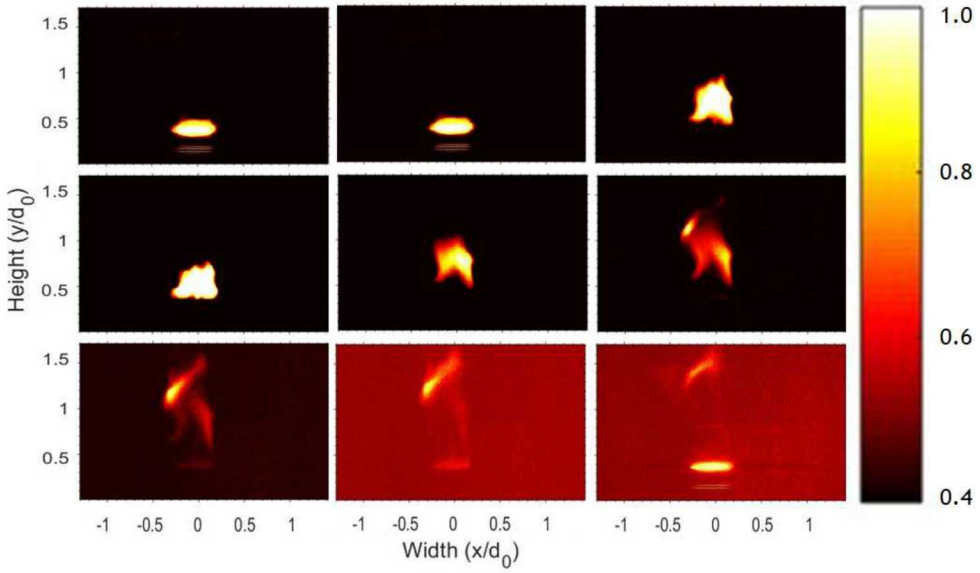

- Plasma is stretched during convection
- Path of convection is repeatable
- Plasma kernel interaction length
  - 300 kHz: 4.8 mm
  - 500 kHz: 3.0 mm

Ultrafast laser-induced breakdown spectroscopy (LIBS)

Variance throughout the burst

$\sigma^2 = 3.8507$

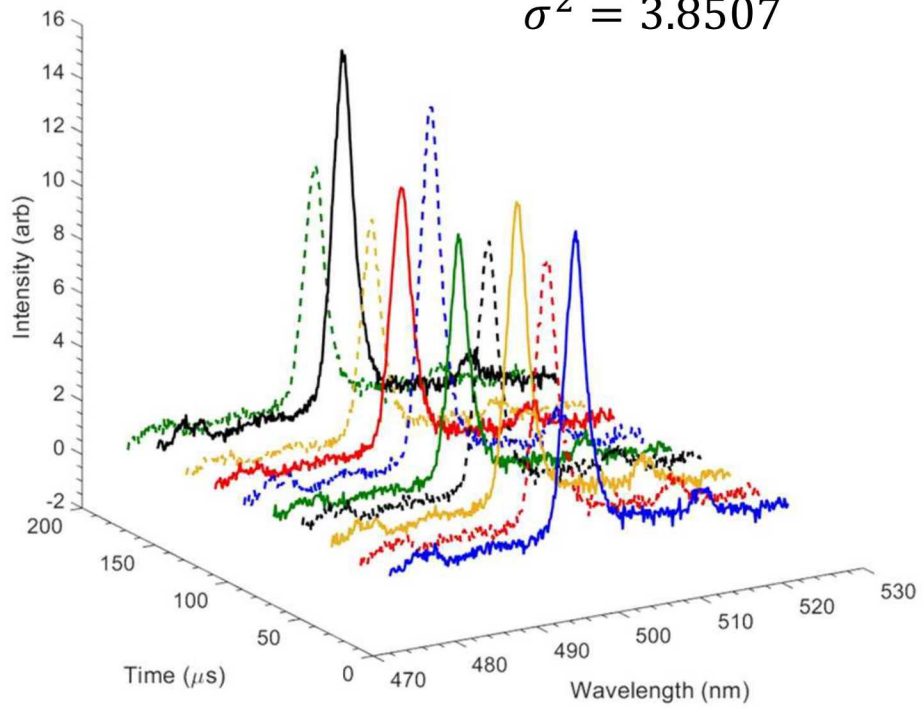

Time evolution of single LIP

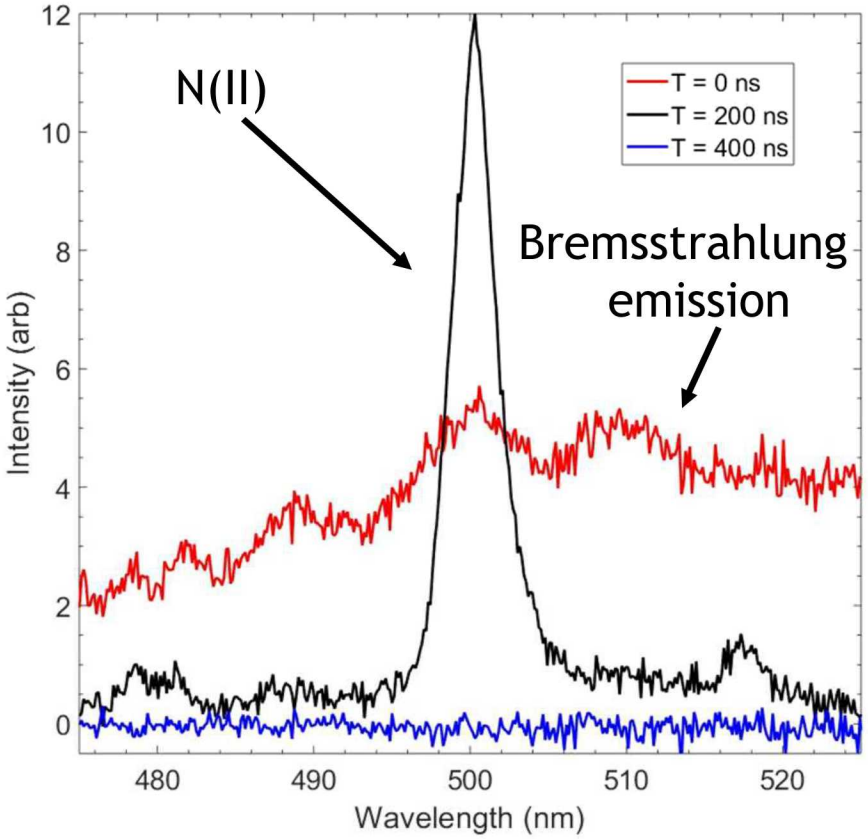

- Plasma varies shot-to-shot throughout burst
- Plasma initially has broadband emission from electron recombination processes
- Strong spectral features appear as plasma is decaying
- By 400 ns after breakdown, plasma no longer emits

Preliminary temperature measurements

N(II) Emission

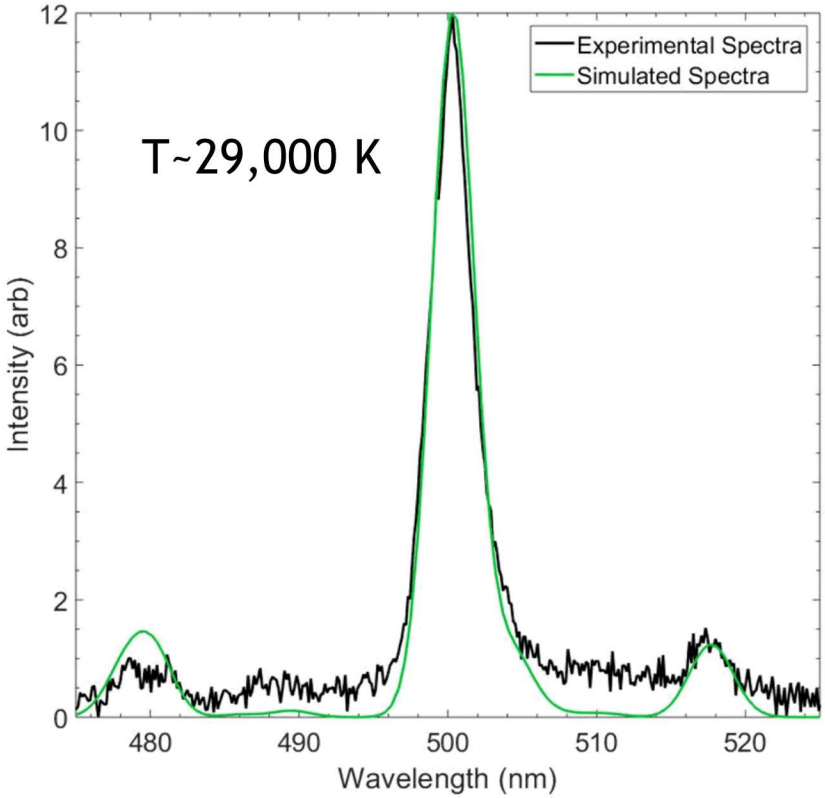

E= 17 mJ/pulse; Burst rate= 500 kHz;
Frame rate = 5 MHz, τ_{exp} = 100 ns

- Spectra was fit using NIST LIBS database
- Chip dispersion ≈ 0.1357 nm/pixel
  - Signal-to-noise tradeoff with resolution
- N_e~ 1e18 cm^{-3}, assumed from previous work
- Peak emission (λ~500 nm) → ^3S, ^5P, ^3D states
  - E_u ~187,000 to 226,000 cm^{-1}
- Secondary emission (λ~518 nm) → $^5P°$, $^5D°$ states
  - E_u~244,000 cm^{-1}
- Sources of uncertainty
  - Only ionized nitrogen present in spectra
  - Raised baseline in fit

Conclusions Part II

- At all repetition rates, the presence of the jet was found to be critical and beneficial to repeatable plasma breakdown.
- Substantial deflection of supersonic, oblique shock waves was achieved with a laser focus prior to the jet, within the jet and on the far side of the jet.
- Increasing pulse energy increased the hot gas core/flow interaction time, but the increase in plasma volume caused a more destructive blast-wave/jet interaction.
- Spectral analysis at E = 130 mJ/ pulse showed strong modulation of the jet in the near field Mach disk and the far field shock train
- N(II) emission imaging at 5 MHz demonstrated a 500 kHz burst could generate a near continuous plasma held in the core flow.
- High burst rate laser-induced plasmas cause permanent, controllable actuation of the flow for the entire burst period, and this actuation has significant implications for non-intrusive, plasma flame holding

Acknowledgements

I gratefully acknowledge DOE's PSAAP-2 Center program for funding my work at the Ohio State University.

I also thank Sandia National Laboratories and the Laboratory Directed Research and Development (LDRD) program for funding this current research

Great thanks for the support and advice from:

- Igor Adamovich
- Zak Eckert
- Kraig Frederickson
- Elijah Jans
- Justin Wagner
- Steven Beresh
- Marley Kunzler
- Seth Spitzer
- Ed DeMauro

Time resolved H atom measurements

H TALIF Line Images

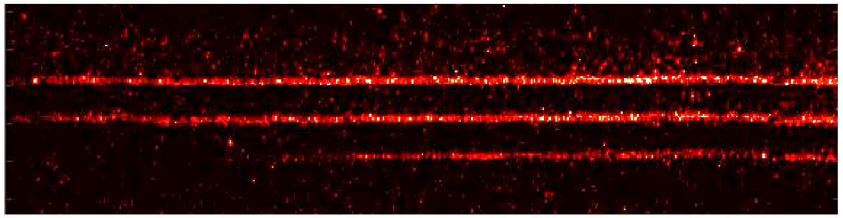

3 μs
300 μs
3 ms

[H] decay after last pulse

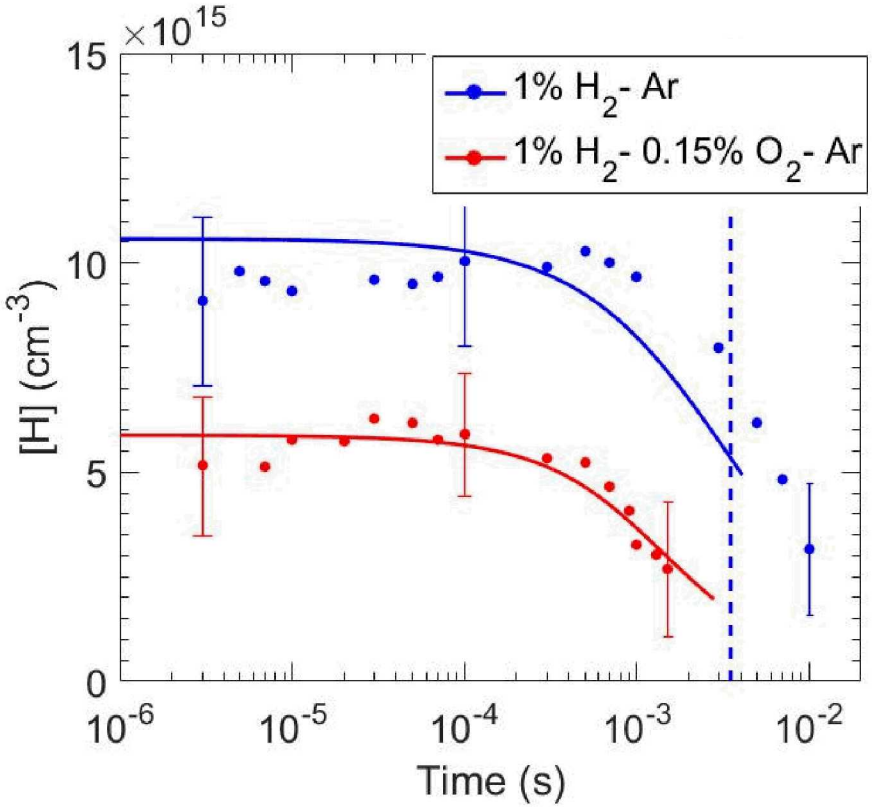

T_0= 500 K, P= 300 Torr 20 kHz, 25 pulses

Kinetic modeling predicts in a 1% H_2 –0.15% O_2 -Ar mixture:

20% of E_{CDP} → H_2 dissociation by Ar* quenching

Goo

16% of E_{CDP} → O_2 dissociation by Ar* quenching,

$$Ar^* + O_2 \rightarrow Ar + O + O$$

H a

36% of H atoms recombine with O_2,

$$H + O_2 + Ar \rightarrow HO_2 + Ar$$

τ_{Con}

Chain branching reactions are minor (~10% of H atom decay) at these low temperatures,

$$H + O_2 \rightarrow OH + O$$

$$\frac{[stable\ products]}{[primary\ radicals]} \approx \frac{[H_2O]}{[H]+[O]} \approx 1.1$$

Nonequilibrium plasmas

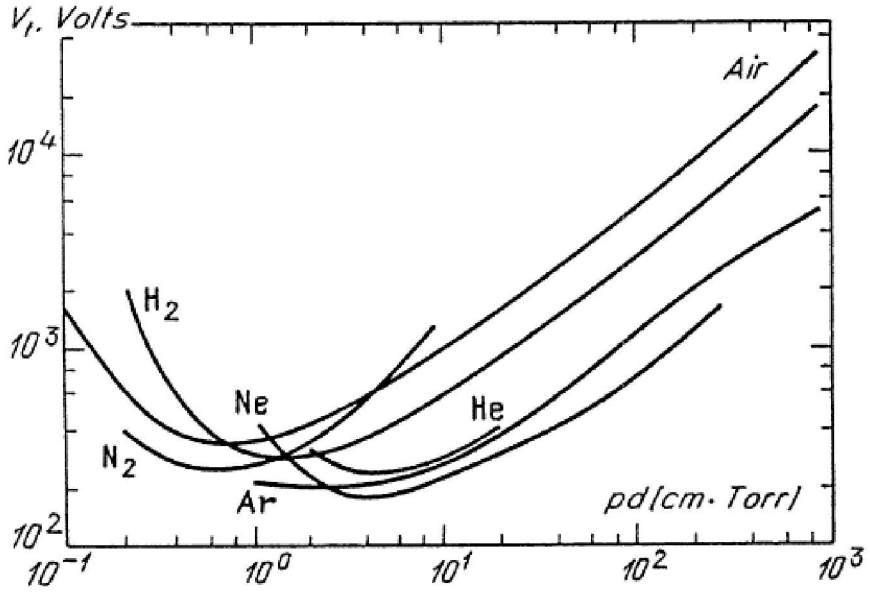

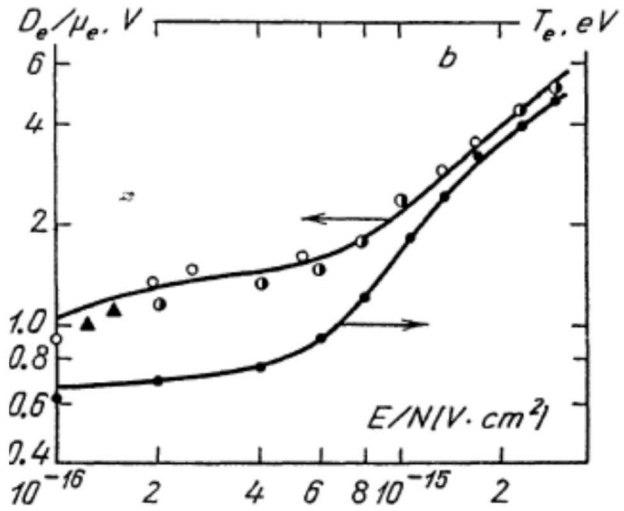

Instability

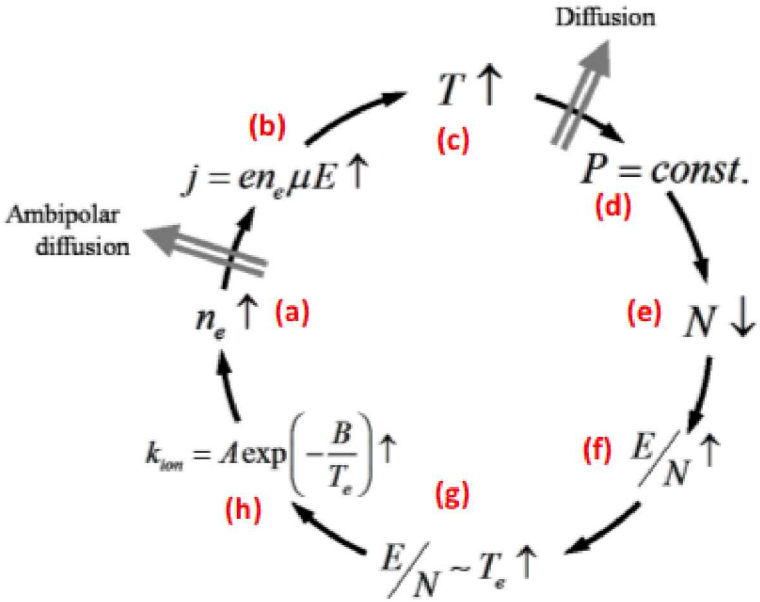

$$\alpha = \frac{k}{\rho C_p} = \frac{kRT}{PC_p}$$

$$D_a = \mu_i \frac{kT_e}{e} \sim T^{1/2}$$

$$\mu_i = \frac{e}{M\nu_m} \qquad \nu_m = N v_T \sigma_c$$

[Ar*] TDLAS measurements to quantify plasma uniformity

Tunable Diode Laser Absorption Spectroscopy (TDLAS)

Ar ($3p^54s$): four states Ar(**$1s_5$**, $1s_4$, **$1s_3$**, $1s_2$)

$$\ln\left(\frac{I}{I_0}\right) = -k(\nu)L$$

$$k(\nu) = \frac{n(l)\phi(\nu)}{C(u,l)}$$

$$C(u,l) = \left(\frac{8\pi}{\lambda^2}\right)\frac{g(l)}{g(u)}A^{-1}(u,l)$$

$$n(l) = \ln\left(\frac{I_0(\nu_0)}{I(\nu_0)}\right)\cdot\frac{C(u,l)}{\phi(\nu_0)L}$$

Energy level diagram for Ar ($3p^54s$) and Ar ($3p^54p$)

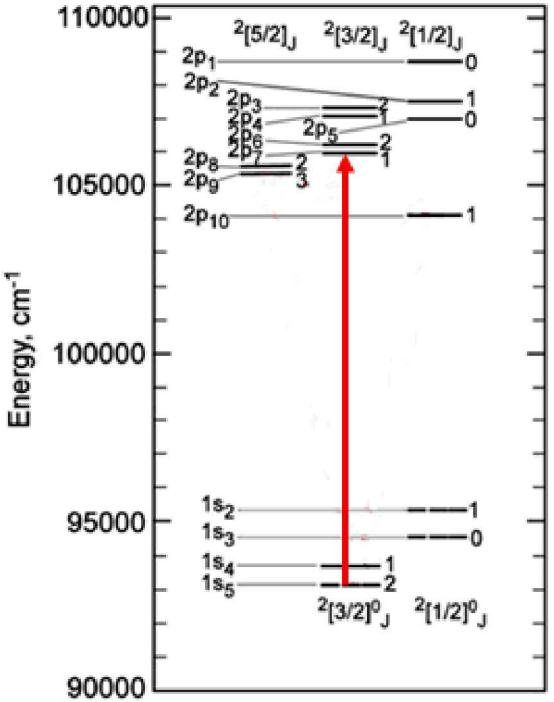

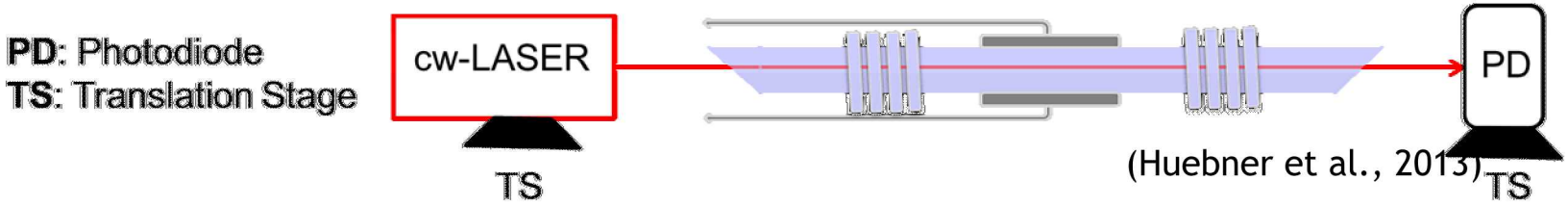

(Huebner et al., 2013)